MP 04W0000274

MITRE PRODUCT

Potential Impact of Carbon Nanotube Reinforced Polymer Composite on Commercial Heavy Aircraft

November 2004

Sarah E. O'Donnell
David B. Smith

Sponsor: MITRE Technology Program
Project No.: 02MSR055-F3
Dept. No.: F052

MITRE
Center for Advanced Aviation System Development
McLean, Virginia

Abstract

This study investigates the possible use of carbon nanotubes as a molecular fiber in a composite material and illustrates the potential impact of incorporating carbon nanotube reinforced polymer (CNRP) composites in a current commercial aircraft. The analysis is performed for a Boeing 747-400 airframe. Theoretical mechanical properties of CNRP are found for single walled carbon nanotube (SWNT) volume fractions (50, 60, and 70%) in high density polyethylene (HDPE). In this simulation, the volume of airframe structural aluminum is replaced with an equivalent volume of SWNT CNRP with no change to the airframe design. Using simulated CNRP-structured airframe weight estimates, a new spread of aircraft operating empty weights (OEW) for the 747-400 is defined and used to predict max takeoff mass, fuel efficiency, operating envelope and flight performance.

The average mass savings of CNRP-structured over aluminum-structured aircraft is 10.07%. The average increase in fuel efficiency from each of the CNRP-structured aircraft categories is 11.2%, with other gains in range, flight duration, increased cruise altitude, and wake mitigation. In general, all notional CNRP 747-400 aircraft analyzed perform approximately equivalent to the lowest mass present day aluminum 747-400.

KEYWORDS: Carbon Nanotube, aircraft composite, aircraft performance

Acknowledgments

The authors wish to extend thanks to Alison Reynolds, Brian Noguchi, Agnieszka Koscielniak, and Jason Giovannelli for their contributions to the project. Thanks to technical advisors Dr. James Ellenbogen, Brigitte Rolfe, David Maroney and Doyle Peed. And special thanks to The MITRE Corporation's Center for Advanced Aviation System Development (CAASD) Chief Engineer, Dr. Glenn Roberts, for initiating the project with Dr. James Ellenbogen and to Charlotte Laqui for her mentorship.

Table of Contents

List of Figures

List of Tables

Section 1

Introduction

Aircraft design favors materials with high specific strengths (strength/density) [1], which reduce aircraft mass while maintaining airframe structural integrity. Many present-day aircraft structures take advantage of the specific strength benefits of aluminum alloys, such as 2024-T3, for the fuselage and graphite-epoxy composites for the empennage and control surfaces. A new composite, reinforced by nanoscopic fibers, may provide aircraft designers with another structural material option for airframes.

The nanoscopic fibers, known as carbon nanotube molecules [2], are a new form of elemental carbon with intriguing properties. For example, the strongest tubes exhibit roughly eighty times the strength, six times the toughness, or Young's Modulus, and one-sixth the density of high carbon steel. Utilizing the carbon nanotube as a molecular "fiber" in a carbon nanotube reinforced polymer (CNRP) provides a potentially favorable material for aerospace applications.

Many present-day commercial aircraft, including the Boeing 747-400, employ graphite-epoxy composites in portions of the airframe [5]. Although commercial aircraft from the Federal Aviation Administration's (FAA) "Heavy" category, such as the 747-400, are primarily structured with aluminum alloys, designs for proposed future aircraft, such as the Boeing 787, include graphite-epoxy composites as the primary structural material [6,7]. The integration of graphite-epoxy composites in airframes may be followed by the utilization of fully CNRP-structured airframes, given the potentially favorable mechanical properties associated with the carbon nanotube molecule.

Carbon fiber composites tend to be less dense than metals, and often provide improved strength and corrosion protection. Carbon nanotube composites will likely provide a low density, corrosion resistant composite that can be used in lower volumes due to the curious mechanical properties of the carbon nanotube, especially its strength, modulus, and conductivity. Incorporating CNRP composites in an airframe potentially offers each of these advantages to the aircraft. Benefits can be seen immediately, without airframe redesign which considers the material strength and modulus properties, by observing the performance and efficiency benefits of weight reduction due to the low density of CNRP.

The analysis presented here considers a notional 747-400 with CNRP as the primary structural material, replacing the entire volume of structural aluminum, without including any modifications to the geometry or design of the airframe. Though such a CNRP-structured 747-400 is unlikely to ever be manufactured, this type of analysis provides insight into a small group of benefits seen by a nano-structured material applied on a macro scale.

This paper discusses the carbon nanotube molecule, its use in a composite material (CNRP), and the potential impacts of CNRP on a current commercial airframe: the Boeing 747-400. First, a brief background on carbon nanotubes is provided. It is followed by a discussion of the theoretical calculations and analysis used to find the mechanical properties of CNRP including Young's Modulus, tensile strength, and density as compared to those found in literature. Using the calculated CNRP mechanical properties, a mass reduction for a 747-400 due to CNRP's specific strength is found. Finally, an analysis is performed of the impact of this mass reduction on the aircraft's performance, fuel consumption, and wake vortex formation.

Section 2

Carbon Nanotube Reinforced Polymer

2.1 The Carbon Nanotube

Some scientists claim the carbon nanotube to be "the strongest material that will ever be made [8]." Pure single-walled nanotubes (SWNT) characteristically exhibit the highest toughness, or Young's modulus, peaking around 1.25 Tera Pascal, (TPa) [4,9,10] (see Figure 2-1). This molecule is tougher than spider silk, whose Young's Modulus nears 300 Mega Pascal, (MPa) [11]. Although both single and multi-walled nanotubes (MWNT) exhibit outstanding strength and modulus, pure SWNT prove exceptional as reinforcing "fibers" for a carbon nanotube reinforced polymer composite [12,14].

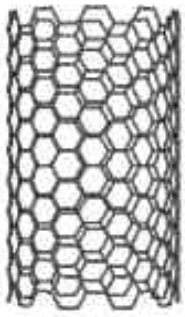

Figure 2-1. Wireframe Model of a Single-Walled Carbon Nanotube Molecular Structure[1]

Carbon nanotubes have various chiralities, or "twists," in the graphene lattice which define the tube structure [15]. The angle of twist is directly related to the chiral vector (C_h) which is defined by the vector addition of two normalized (unit) vectors, $\mathbf{a_1}$ and $\mathbf{a_2}$, and their respective indices (m,n) as shown in the following equation:

$$\mathbf{(1)}\quad \mathbf{C_h} = n\mathbf{a_1} + m\mathbf{a_2}$$

Because mechanical properties of the (10,10) armchair carbon nanotube have been theoretically [19] and experimentally [3,4] observed, it is the molecular nanotube of choice for this analysis. Figure 2-2 illustrates the chiral vector for an armchair nanotube, where m = n = 10. The name "armchair" originates from the geometry of the nanotube bonds around the tube circumference.

---

[1] Notice the chicken-wire like lattice structure of what appears to be a graphene sheet rolled into a tubule.

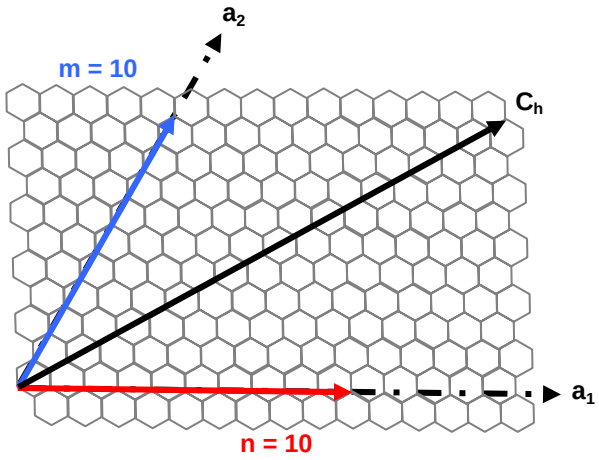

Figure 2-2. (10,10) Armchair Nanotube Chiral Vector Diagram[2]

Armchair SWNTs behave as metals [16,17]. Conductivity in metallic nanotubes occurs via ballistic electron transport, resulting in high current carrying capacity with little energy sacrifice to heat [18].

The Young's Modulus for a (10,10) armchair SWNT averages approximately 640 GigaPascal (GPa) according to calculations [19] and measurements [3]. SWNT bundles exhibit tensile strengths that range from approximately 15 to 52 GPa and a corresponding tensile strain minimum of 5.3%, where the load is applied to the nanotubes at the perimeter of each bundle [3,20]. Multi-walled nanotubes range in tensile strength from 11 to 63 GPa, with a tensile strain at fracture [21,22] of close to 12%.

2.2 Carbon Nanotube Reinforced Polymer Composite

Classically, composites consist of a high-modulus fiber in a low-modulus matrix, where the fiber toughens and strengthens the binding material, or matrix. Due to their exceptional mechanical properties, (10,10) SWNT are commonly used as the reinforcing fiber in carbon nanotube composite [12,14], and will be used for the CNRP property estimates to follow.

In this analysis, the density, tensile strength, and Young's Modulus are known for the polymer matrix and the nanotube molecule. The following analysis includes high density polyethylene (HDPE) as the polymer matrix material, or low modulus phase, and (10,10) SWNT as the high modulus phase. The material properties of HDPE and SWNT are listed in Table 2-1.

---

[2] A formed (10,10) armchair carbon nanotube appears as a tube rolled seamlessly along the Ch. The Ch shows the direction of "twist" and circumference of the tubular structure.

Table 2-1. Mechanical Properties of High-and Low-Modulus Phases of CNRP[3]

Material Type	Density (kg/m^3)	Young's Modulus (Gpa)	Tensile Strength (Gpa)
HDPE[23]	955	2.40	0.021
<SWNT>[9,19,3]	1300	640	37.0
SWNT[9,4,3]	1300	1200	50.0

Several methods exist for calculating mechanical properties of composites, including the method of mixtures (MOM) [1,2,5]. MOM is used as a first order approximation in this research [26] to estimate the density, tensile strength, and Young's Modulus of bi-directional CNRP. The evenly aligned, dispersed fibers of a bi-directional composite, illustrated in Figure 2-3, fall under the category of a uniformly dispersed, aggregate composite commonly analyzed by MOM [1,25,27]. MOM enables the analysis of materials on the macro-scale when given the bulk mechanical properties, including tensile strength, modulus, diffusivity, thermal conductivity, or electrical conductivity [1] of the composite's constituents.

[3] High-Density Polyethylene serves as the low modulus phase, and Single-Walled Carbon Nanotube as the high-modulus phase. For more conservative calculations, the mean values of mechanical properties of SWNT are used in this analysis, denoted by <SWNT>. Optimal values for SWNT are also presented.

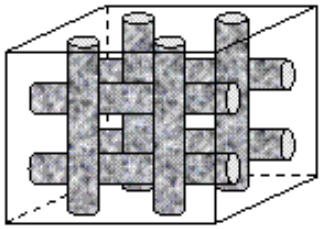

Figure 2-3. Bi-Directional Composite Structure[4]

The general equation for the method of mixtures is:

$$\mathbf{(2)}\quad X_{composite} = \left[V_{fiber} X_{fiber}^{\alpha} + \left(1 - V_{fiber}\right) X_{matrix}^{\alpha}\right]^{1/\alpha}$$

where V is volume fraction, X is the mechanical property, and α is the stress index [1]. The CNRP mechanical property analysis includes a range of three SWNT volume fractions: 50, 60, and 70% in HDPE. Present-day, commercially available common graphite-epoxy composite consists of 66-70% volume fraction graphite fibers in epoxy [27].

Evaluating at $\alpha = 1$, indicates a unidirectional composite where the force is applied parallel to the axis of the fibers, placing the material in isostrain as illustrated in Figure 2-4a. Evaluating at $\alpha = -1$ indicates a unidirectional composite where the force is applied orthogonal to the axis of the fiber orientation, placing the material in isostress as illustrated in Figure 2-4b. Evaluating equation (1) within boundary values, $-1 < \alpha < 1$, produces mechanical property estimates for a bidirectional composite with orthogonally oriented fibers as seen in Figure 2-3, existing in the isostrain and isostress condition with the load applied on either fiber orientation axis.

---

[4] The reinforcing fibers are oriented at 0° and 90° in the polymer matrix.

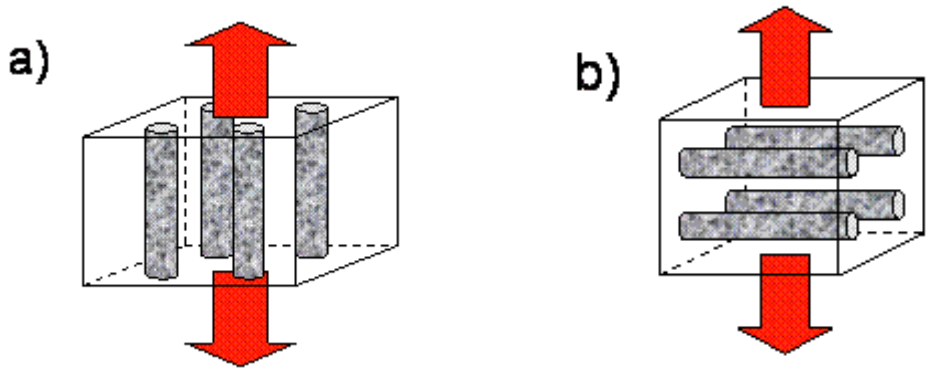

Figure 2-4. Composite Axial Loading[5]

Evaluating Equation (1) for Young's Modulus, tensile strength, and density at $\alpha = 0.01$ provides a first order approximation for a bi-directional composite of orthogonal fiber orientation with a higher-modulus fiber in a lower-modulus matrix [1]. As seen in Table 2-2, the following results are for the SWNT volume fractions, producing a range of results for bi-directional CNRP used in the aircraft structure analysis in Section 3.

Table 2-2. CNRP Mechanical Properties at Selected Single Walled Carbon Nanotube Volume Fractions[6]

CNRP % SWNT	Density (kg/m^3)	Young's Modulus (Gpa)	Tensile Strength (Mpa)
50	1130	57.6	1740
60	1160	97.9	3470
70	1200	162	6620

Experimental CNRP findings by other investigators show consistent values for material mechanical properties vary [32,35] due to several factors, including experimental apparatus, SWNT dimensions, SWNT density measurement, the ability to uniformly disperse nanotubes throughout the matrix, and differences in the purity of SWNT [35]. Some investigators have

---

[5] a) Unidirectional composite in isostrain. The uniaxial load is applied parallel to the reinforcing fibers.
b) unidirectional composite in isostress. The uniaxial load is applied orthogonal to the reinforcing fibers.

[6] CNRP constituent properties are found in Table 1. HDPE is the low-modulus matrix phase and CNRP is the high-modulus "fiber" phase.

been focusing on spinning the nanotube molecules into fibers, much as spiders spin silk, to weave fabrics used in composite laminate layers [36,38]. Many of these same findings exhibit only slight improvement over the mechanical properties of current carbon fiber composites [32].

As dispersion becomes more uniform and isolating SWNT from bundles does not affect their purity, experimental CNRP properties will potentially approach those predicted theoretically, providing improved values over the results illustrated in the first order approximation in this study and more accurate continuum and constitutive models from other studies. Such a possible improvement over current structural materials, shown in Table 2-3, might mean that CNRP will replace existing alloys and composites without compromising added weight for strength and toughness, leading to improvements in the performance of the vehicles which use CNRP in their structures.

Table 2-3. Mechanical Properties of Common Structural Materials[7]

Material Type	Density (kg/m^3)	Young's Modulus (Gpa)	Tensile Strength (Mpa)
Steel	7845	200	620
Titanium	4820	110	1170
Aluminum	2780	73	480
CFRP[8]	1600	181	1500

[7] AISI 1040 rolled steel [28]; Ti-13V-11Cr-3Al solution treated, Age 4500°C Titanium [29] (used on SR-71 Blackbird [30]); 2024-T3 Aluminum [31]; Thornel 300 graphite fibers in Narmco 5208 Epoxy for T300/5208 DFRP [27].

[8] Carbon Fiber Reinforced Polymer.

Section 3

Mass Analysis of CNRP-Structured Aircraft

Using CNRP in aircraft structures has several predictable impacts on aircraft design. The most obvious of which is significant airframe weight reduction stemming from CNRP's low density and complemented by its high strength and modulus presented in Table 2-1. To demonstrate this potential, a notional CNRP-structured present day Boeing 747-400 commercial airframe is analyzed.

It is understood that re-constructing present-day aircraft with CNRP airframes is a highly unlikely future scenario. However, because future aircraft designs remain uncertain, examining the impact CNRP may have on today's aircraft provides insight into potential future aircraft performance and designs.

To illustrate the likely impact of reduced 747-400 airframe weight from utilizing CNRP, the volume of structural aluminum in the 747-400 is replaced with an equivalent volume of CNRP. Multiplying the 66,150 kg mass of 2024-T3 aluminum, a common material used in commercial jet aircraft [30], in the 747-400 structure [39] by its density provides the volume of structural material considered in the analysis. The mass of CNRP is determined by multiplying the volume of structural material by the density of CNRP. This calculation is performed for three SWNT volume fraction-dependent densities to obtain three structural CNRP masses. Although a lower volume of CNRP would likely exist because of its strength and resilience, this analysis does not account for the re-design of specific structural elements involved. Other structural characteristics, especially airfoil and fuselage geometry, remain as found in the original aircraft and as described by Boeing [40] in the 747-400 Document D6-58326-1.

The evaluation to follow applies the assumptions and structural mass projections for the notional CNRP-structured 747-400 included above to an aircraft mass analysis. In Section 4, performance characteristics, such as fuel efficiency, aircraft range, flight duration, cruise altitude, and vortex circulation resulting from the change in aircraft mass are evaluated and discussed.

The mass reduction analysis compares mass at takeoff (M_{AT}) values from the original 747-400 to calculated CNRP M_{AT} values. Boeing document [40] D6-58326-1 provides five sets of aircraft mass data for the current 747-400 powered by PW-4056 engines. From the five available data sets, the lowest, moderate, and highest mass data were chosen for use in this study. Each data set includes M_{AT}, operating empty weight (OEW or M_{OE}), maximum payload (M_L), and maximum fuel load (M_F). OEW is the only value that remains constant (179,015 kg) for the low, moderate, and high present-day 747-400 aircraft masses. It includes "the weight of the structure, powerplant, furnishing systems, unusable fuel and other

unusable propulsion agents, and other items of equipment that are considered an integral part of a particular airplane configuration." The fuel and payload are the primary contributors to the mass differentiation in Boeing's mass data sets. Zero fuel weight (ZFW) might similarly be affected, from an operational standpoint, to permit an increase in payload directly proportional to the decrease in aircraft mass due to CNRP construction, but is not addressed in this paper.

As the actual airframe geometry remains the same, M_{AT} is considered. It is unlikely that contemporary airframes would use a new material such as CNRP without modifications; therefore the redesign and associated efficiency analysis would include maximum mass at takeoff (M_{TO}). M_{TO} is a design criteria and is limited by aircraft strength and airworthiness requirements [40]. Thus, a CNRP-structured airframe with less material for the same loading or the same amount of material with higher load tolerance would have a different M_{TO} to consider.

The CNRP aircraft mass analysis is based on the low, moderate, and high 747-400 data as well as the CNRP material property results from the previous section. To calculate the range of CNRP M_{AT}, the CNRP OEW [40] are found for each of the SWNT volume fractions. This calculation subtracts the mass of structural aluminum, and adds in each of the three new CNRP masses to obtain a range of CNRP OEWs shown in Table 3-1.

Table 3-1. Range of CNRP 747-400 Operating Empty Weights

Material	OEW (kg)
Aluminum	179,015
50% SWNT CNRP	139,800
60% SWNT CNRP	140,600
70% SWNT CNRP	**141,400**

Then, for each of the OEWs calculated, the low, moderate, and high Boeing data are applied using the following equation [41]:

$$\textbf{(3)}\quad M_{AT} = M_{OE} + M_F + M_L$$

to obtain a matrix of possible CNRP M_{AT} shown in Table 3-2. This matrix of CNRP structured aircraft takeoff masses is applied to the performance and efficiency analysis.

Table 3-2 illustrates CNRP structured 747-400 M_{AT} ranges for low, moderate, and high masses at increasing SWNT volume fractions as compared to the original aluminum-structured 747-400 for low, moderate and high as found in Boeing Document D6-58326-1. CNRP M_{AT} of the low range average 10.58% mass savings over the low aluminum M_{AT}. CNRP M_{AT} of the moderate range average 9.96% mass savings over the moderate aluminum

M_{AT}. CNRP M_{AT} of the high range average 9.67% mass savings over the high aluminum M_{AT}. This exhibits an average mass savings of 10.07% for all CNRP M_{AT} over aluminum M_{AT}.

Table 3-2. CNRP 747-400 M_{AT} (kg) Matrix

	747-400 Structural Material			
	Aluminum *2024-T3*	**CNRP** *50% SWNT*	*60% SWNT*	*70% SWNT*
Low Mass	362,874	323,600	324,500	325,300
Moderate Mass	385,554	346,300	347,200	348,000
High Mass	396,894	357,700	358,500	359,300

The results of the initial mass analysis provides a range of nine potential CNRP-structured 747-400 estimates, from the high M_{AT} low volume fraction option to the low M_{AT} high volume fraction option.

Section 4

CNRP Aircraft Performance

Weight reduction directly affects aircraft performance, economics, and efficiency. This should be true, even assuming no change in aircraft geometry. To test this thesis with regards to CNRP-structured airframes, several further analyses are performed. First, fuel efficiency and aircraft range are analyzed for both aluminum and CNRP 747-400 airframes. Then, the flight operating envelopes are compared and analyzed. Finally, wake vortex formation and behavior estimate is performed. For the analysis, the Pratt & Whitney 4056 turbofan, a typical Boeing 747-400 engine, is considered in both present-day and notional CNRP-structured aircraft.

4.1 Fuel Considerations

The fuel efficiency analysis utilizes a United Airlines handbook for 747-400 flight operations [42]. The first part of the fuel efficiency analysis requires an estimation of the fuel consumption upon ascent. Subtracting this fuel volume from the takeoff weight provides an initial aircraft weight at the start of cruise. The analysis of a cost-indexed step climb cruise follows, where a predetermined weight of fuel is burned per altitude step [42]. Fuel efficiency and aircraft range improvements are derived from the cruise portion of this analysis.

4.1.1 Ascent Fuel Burn

For purposes of this analysis, the cruise regime is considered to begin at 30,000 ft, with ascent between 0 and 30,000 ft. The calculations for ascent are made from 0 to 30,000 ft over five altitude intervals. At each of these intervals, the flight operations manual [42] provides airspeed and fuel consumption data, which is assumed constant over the interval. Given the typical 747-400 aircraft ascent rate of 3,000 ft/min (15.25 m/s) [43], the flight duration over each altitude interval during ascent is found. The fuel mass consumed at each interval for the duration of ascent is calculated by multiplying the interval duration by the fuel mass flow rate. Summing over each interval for fuel mass consumed produces a fuel consumption figure for ascent, roughly 5,000 kg (+/- 650kg).

It is understood that fuel consumption during may reach or exceed 10,000 kg, depending on the pilot and flight circumstances. For this analysis, however, the 5000 kg fuel consumption during ascent is used for present-day and CNRP aircraft. The primary gain in fuel consumption reduction will likely be observed over the course of cruise of several hours, not an ascent of several minutes. The 5,000 kg of fuel burned upon ascent is subtracted from the fuel mass upon takeoff for each of the M_{AT} of the aircraft analyzed, providing new

weight matrices for the cruise analysis. The new matrix is Table 3-2 with each entry minus 5,000 kg.

4.1.2 Cruise Fuel Burn

Fuel consumption analysis at the cruise regime provides a glimpse of higher altitudes and longer ranges for the same initial fuel load for each aircraft. The aircraft is assumed to fly a cost-indexed step cruise where each aircraft analyzed burns 20,000 lbs of fuel at each step over the course of 180,000 lbs of consumed fuel. Fuel burn charts from United Airlines for a four-engine Cost Index = 100 step cruise are used for the analysis. The charts provide optimum fuel consumption, true airspeed (TAS), Mach, and engine pressure ratios (EPR) and flight level (altitude) per aircraft weight at that altitude. Descent is not considered in the analysis.

4.1.3 Operational Performance

A comparison of the cost-indexed cruise aircraft performance results including fuel efficiency, range, flight duration, and peak cruise altitude are shown in Table 4-1. Fuel efficiency is expressed in nautical miles (NAM) per 1,000 lbs of fuel burned, the aircraft range in NAM, the duration of the cruise in hours, and the peak altitude during the cruise in feet. The data shows results for present-day and CNRP-structured 747-400.

Increases in fuel efficiency as well as range in CNRP-structured 747-400 over present-day 747-4000 are illustrated in Figures 4-1 and 4-2, respectively. Each of the charts compare the CNRP-structured 747-400 performance to the present day 747-400 low, moderate, and high 747-400 mass data from the Boeing document D6-58326-1. In the charts, Low 50% signifies the CNRP 747-400 at the low M_{AT} with CNRP of 50% SWNT.

Table 4-1. Cost-Indexed Cruise Performance Comparison[9]

		Avg Fuel Efficiency NAM/1000lbs	Range (NAM)	Duration (hours)	Peak Cruise Altitude (ft)
Current 747-400	***Low***	21.32	3,861	7.88	37,000
	Mod	19.72	3,569	7.24	35,000
	Hi	19.24	3,480	7.05	34,000
Notional CNRP-Structured 747-400	***Low 50%***	23.89	4,348	8.88	39,000
	Low 60%	23.89	4,348	8.88	39,000
	Low 70%	23.89	4,348	8.88	39,000
	Mod 50%	21.92	3,969	8.11	37,000
	Mod 60%	21.92	3,969	8.11	37,000
	Mod 70%	21.92	3,969	8.11	37,000
	Hi 50%	21.32	3,861	7.88	37,000
	Hi 60%	21.32	3,861	7.88	37,000
	Hi 70%	20.76	3,752	7.66	36,000

From an analysis of the results illustrated in Table 4-1, CNRP aircraft of low M_{AT}, regardless of SWNT volume fraction in CNRP, exhibit 12% increase in fuel efficiency, 487 NAM longer range, 1 hour longer flight duration, and they cruise 2,000 ft higher than current low mass 747-400. CNRP aircraft from the moderate M_{AT} range exhibit 11% increase in fuel efficiency, 400 NAM longer range, 0.87 hour longer flight duration, and cruise at 2,000 ft higher than current 747-400 from the moderate M_{AT} range. CNRP aircraft from the high M_{AT} range exhibited a 10% increase in fuel efficiency, 345 NAM increase in range, and cruise 2,000 ft higher than current 747-400 from the high M_{AT} range, with a 0.76 hour increase in duration of flight.

9 Present-day and CNRP-structured 747-400 results based on Cost-Indexed Cruise Tables in the United Airlines 747-400 Flight Manual. Given aircraft mass, the manual provides optimal fuel consumption and altitude. Flight range and duration were derived from the fuel consumption, assuming the aircraft burns 20,000 lbs of fuel per "step".

An interesting observation from Figures 4-1 and 4-2 is that a low mass CNRP-structured 747-400 of 50% SWNT CNRP exhibits results similar to the 60% and 70% SWNT CNRP airframes. This is due to the minimal impact an increase in SWNT volume fraction has on the composite material density between 50% and 70% SWNT. The slight increase in mass due to an increase in SWNT volume fraction is small enough to be negligible in the mass of the aircraft when using the United Airlines flight manual tables for efficiency in a cost-indexed cruise. The case is the same for the moderate and partially for the high mass CNRP airframes.

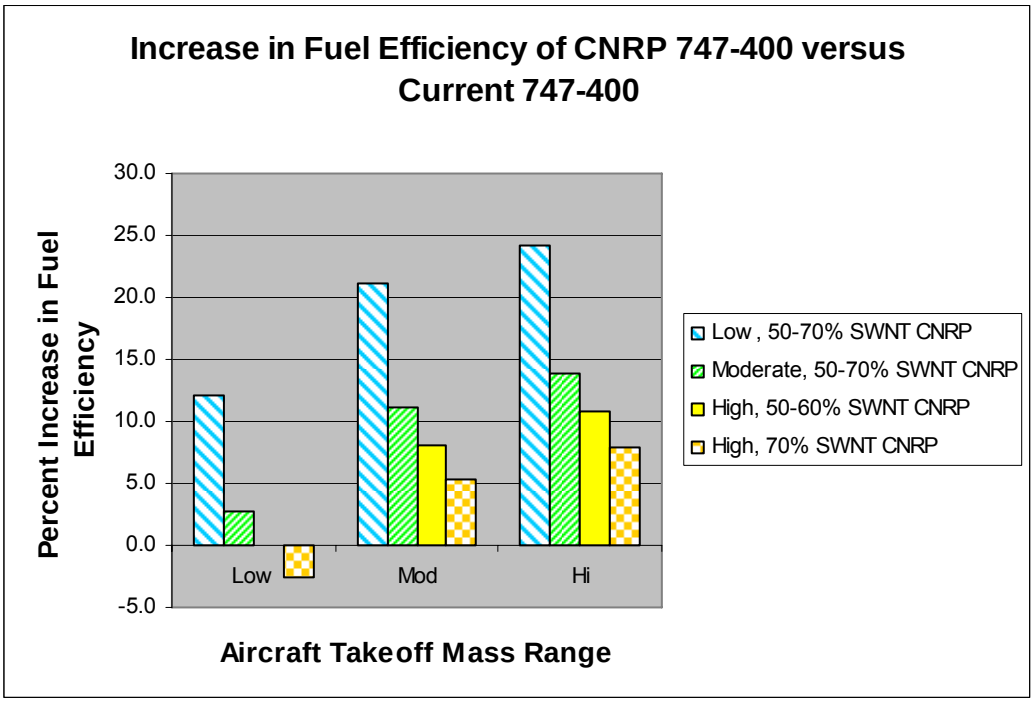

Figure 4-1. CNRP 747-400 Percent Increase in Fuel Efficiency[10]

[10] Fuel efficiency of notional CNRP-structured 747-400 from 50, 60, and 70% SWNT CNRP at low, moderate, and high masses for each SWNT percentage are compared to the fuel efficiencies of low, moderate, and high mass present-day 747-400.

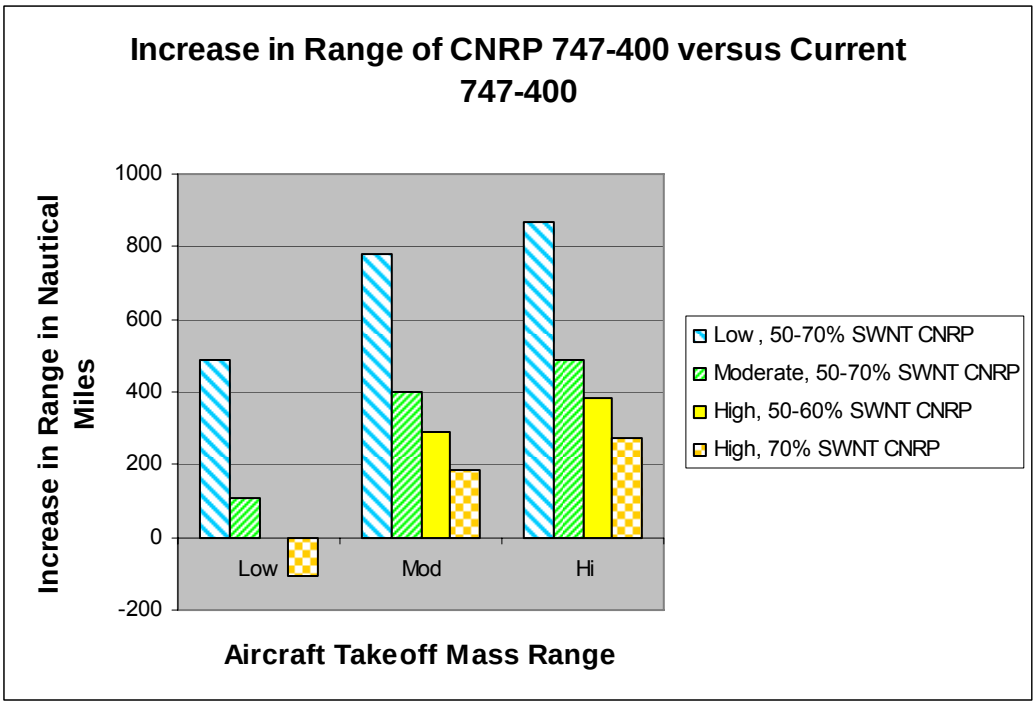

Figure 4-2. CNRP 747-400 Increase in Flight Range in Nautical Miles[11]

Although there is little difference in fuel consumption, flight range, duration, and cruise altitude due to increased SWNT volume fraction percentage *within* an individual CNRP mass category (low, moderate, or high), there are differences *between* the low, moderate, and high CNRP mass categories. Significant differences exist between the low, moderate, and high CNRP aircraft and the original low, moderate, and high present-day aircraft as seen in Figures 4-1 and 4-2. The low CNRP-structured 747-400 of 50-70% SWNT illustrates the most dramatic improvements, with 12-24% increase in fuel efficiency and 490-870 NAM flight range increase when compared to the low-high original aircraft.

The high mass 50-70% SWNT CNRP-structured airframe performs in a manner nearly equivalent to the low mass aluminum-structured airframe, step climbing through cruise from 30,000 to 37,000 ft and traversing 3,861 NAM. This is an improvement of 381 NAM more than the high mass aluminum-structured airframe, illustrating that the weight reduction of CNRP in a high-mass category airframe places the new airframe in the low mass category.

---

[11] Flight range of notional CNRP-structured 747-400 from 50, 60, and 70% SWNT CNRP at low, moderate, and high masses for each SWNT percentage are compared to the flight range of low, moderate, and high mass present-day 747-400.

This result illustrates the potential increase in mass moved per nautical mile, as increase in mass sets is post-OEW for typical aluminum 747-400, meaning the cargo from a typical high mass aluminum 747-400 can be flown at the typical low mass aluminum 747-400 scale with a high mass CNRP 747-400. This should permit the CNRP-structured aircraft to carry more cargo at a lower cost because the weight saved in structural mass could be replaced with cargo mass.

Another interesting result that appears in Table 4-1 is the low mass 50-70% SWNT CNRP-structured aircraft which cruise at 39,000 ft, traverse 4,348 NAM with 12-24% improvement in fuel efficiency over aluminum-structured 747-400s. Translating this efficiency to cost savings, for a trans-Continental U. S. flight, 3,000-5,300 gallons of fuel is conserved, saving $2,700-$4,770 in fuel cost, assuming $0.90/gallon for Jet A fuel [44].

The results of this analysis present an incomplete picture of the impact of CNRP because they only deal with efficiencies gained from a weight savings and do not include potential gains from aircraft redesign. The latter takes advantage of the increase in material strength and toughness.

4.2 Flight Performance

Evaluating an aircraft's operating envelope provides several critical velocities over the aircraft's range of altitudes. The velocity profiles include maximum, minimum, and stall velocity, with considerations for mach drag rise, best range, best climb, and best angle of climb velocity. Table 4-2 presents these velocities evaluated at the final altitude step (from Table 4-1) in the cost-indexed cruise, when the aircraft had each depleted 180,000 lbs of fuel. This is calculated for low, moderate, and high mass aluminum-structured 747-400 as well as low, moderate and high mass, CNRP-structured 747-400 of 50-70% SWNT CNRP. Aircraft performance analysis equations used to obtain the results in Table 4-2 are adapted from those in several standard aircraft design texts [30,41,45] to determine maximum velocity (V_{max}), minimum velocity (V_{min}), stall speed (V_{stall}), and thrust required (T_R). These equations are as follows:

$$\textbf{(4)}\quad V_{max} = \sqrt{\left[\left(\frac{\frac{T_a}{S}}{\rho_{SL}\sigma C_{DO}}\right)\left(1+\sqrt{1-\frac{4KC_{DO}}{\frac{T_a}{M}}}\right)\right]}$$

$$\textbf{(5)}\quad V_{min} = \sqrt{\left[\left(\frac{\frac{T_a}{S}}{\rho_{SL}\sigma C_{DO}}\right)\left(1-\sqrt{1-\frac{4KC_{DO}}{\frac{T_a}{M}}}\right)\right]}$$

$$\textbf{(6)}\ V_{stall} = \sqrt{\left[\left(\frac{2M}{\rho_{SL}\sigma S Cl_{\max}}\right)\right]}$$

$$\textbf{(7)}\ T_R = \left(0.5\rho_{SL}\sigma V_{cruise}^2 S C_{DO}\right) + \left(\frac{2KM^2}{0.5\rho_{SL}\sigma V_{cruise}^2 S}\right)$$

using available thrust (T_a), wing area (S), air density at sea level (ρ_{SL}), density ratio (σ), zero lift-drag coefficient (C_{DO}), drag due to lift factor (K), aircraft mass (M), and maximum coefficient of lift (Cl_{max}).

For each of the aircraft discussed in the operational performance section, the flight performance deviated very little from aircraft to aircraft. Table 4-2 shows cruise velocities each around 490 kts, max velocities around 755 kts, minimum velocities around 243 kts, stall velocities around 194 kts, and 62,000 lbs average thrust required. The low mass CNRP aircraft require approximately 10,000 lb less thrust than the low mass aluminum aircraft counterpart. Similarly, 10,000 lb less thrust required also is seen in the case of the moderate CNRP – moderate aluminum aircraft mass, and the high CNRP – high aluminum aircraft mass comparisons, as well.

Table 4-2. CNRP 747-Flight Performance Comparisons (180,000 lb fuel consumed)

		Cruise Velocity (knots)	Max Velocity (knots)	Min Velocity (knots)	Stall Velocity (knots)	Thrust Req'd (lbs)
Current 747-400	***Low***	490	756	242	193	64,120
	Mod	493	747	255	197	69,565
	Hi	494	742	256	209	72,174
Notional CNRP-Structured 747-400	***Low 50%***	490	758	238	192	54,972
	Low 60%	490	757	239	192	55,174
	Low 70%	490	757	240	192	55,389
	Mod 50%	489	758	237	191	60,230
	Mod 60%	489	758	238	191	60,432
	Mod 70%	489	758	239	192	60,645
	Hi 50%	490	758	237	191	62,840
	Hi 60%	490	757	237	191	63,041
	Hi 70%	490	757	238	191	63,242

The high mass CNRP-structured aircraft stalls at nearly 20 kts less than high mass aluminum-structured aircraft. The low mass aluminum aircraft and the low mass CNRP aircraft have approximately 758 kt maximum velocity, 237 kt minimum velocity, 191 kt stall speed, and cruise at 0.854 Mach.

The flight performance results for CNRP-structured 747-400 aircraft remain relatively consistent with present-day 747-400s in part due to the use of current 747-400 flight manuals for evaluating the flight performance of both airframe types; therefore, results will not fall far outside of the current 747-400 operating envelope. Performance gains might be more dramatic if the aircraft were to undergo redesign leveraging the advantages potentially available with CNRP, such as its strength and Young's Modulus. Redesigning specific portions of the airframe may significantly reduce the mass further than can be shown in this analysis.

Evident in equations (4) and (5), maximum and minimum velocity changes to the fourth root of a change in mass. The stall velocity given in equation (6) changes as the square root of the change in mass, leaving thrust required as the only result which changes with the square of aircraft mass. From equations (4), (5), and (6) it is evident that significant effects of small to moderate weight reduction on aircraft performance are more evident in available and required thrust, T_A and T_R respectively.

4.3 Wake Vortex Behavior

A lighter aircraft requires less lift to remain airborne and also produces less intense wake turbulence. Wake vortices, two counter-rotating tornado-like phenomena, occur as an inherent byproduct of lift [46]. (See Figure 4-3.)

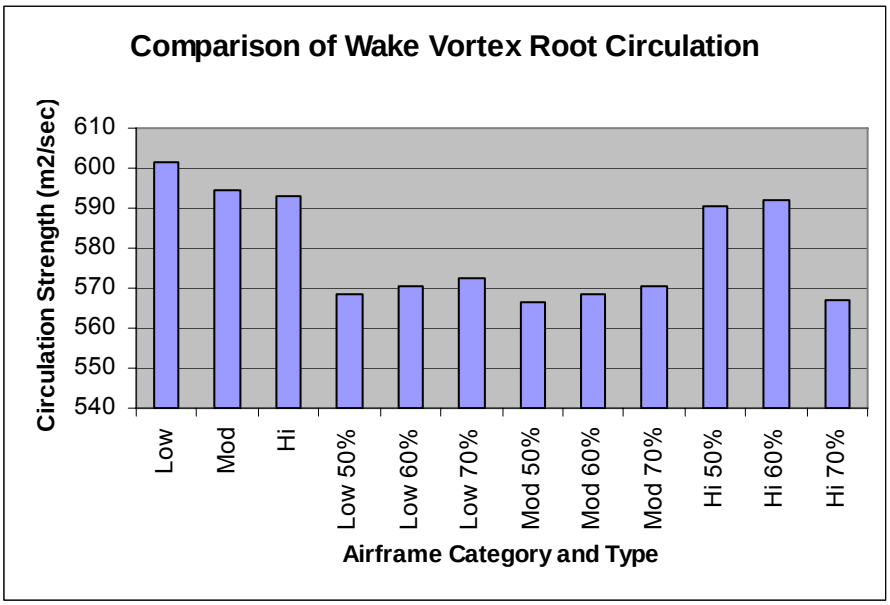

Figure 4-3. CNRP 747-Wake Vortex Comparisons (180,000 lb fuel consumed)12

The vortex behavior results for CNRP-structured and aluminum-structured 747-400 follows the same pattern illustrated in the aircraft performance analysis, with the CNRP structured aircraft vortex behaviors closely linked to the low mass aluminum-structured aircraft vortex behavior. The vortex root circulation (Γ_o), core separation (b_o), and sink velocity (v_o) are calculated with the respective equations [47,48]:

12 Wake strengths of notional CNRP-structured 747-400 from 50, 60, and 70% SWNT CNRP at low, moderate, and high masses for each SWNT percentage are compared to the wake strengths of low, moderate, and high mass present-day 747-400.

$$\textbf{(8)}\ \Gamma_o = \frac{4Mg}{\pi\rho B V_{cruise}}$$

$$\textbf{(9)}\ b_o = sB$$

$$\textbf{(10)}\ v_o = \frac{\Gamma_o}{2\pi b_o}$$

Independent parameters in equations (8), (9), and (10) are aircraft mass (M), gravitational constant (g), air density (ρ), wingspan (B), cruise velocity (V_{cruise}), and elliptical wing load scaling factor (s).

Each of the CNRP structured aircraft exhibit root circulation of approximately 570 m^2/s (6,040 ft^2/s) illustrated in Figure 4-3, which is approximately 5% less than the aluminum aircraft. Upon conception, the vortex cores are 50.96 m (167.2 ft) apart for each aircraft as the wingspan remains constant throughout the analysis. Vortex descent rates are consistently between 1.80-1.90 m/s (5.85-6.17 ft/s) upon conception.

Section 5

Discussion

To scale the complexity of the analysis, it was necessary to omit from consideration several factors which might have substantial impact on the results in a more detailed analysis. These include consideration of the molecular interactions of carbon nanotubes with the polymer matrix, utilizing the multifunctionality of the carbon nanotube (such as strength and modulus, as well as electrical and heat conductivity), constraints that might be imposed in FAA certification and approval of such a unique material for application to aircraft designs, the effects of aircraft redesign leveraging all the favorable mechanical properties of CNRP, and aircraft performance in the National Airspace System (NAS).

The aircraft performance analysis illustrated in this paper shows the optimum altitude and associated performance characteristics for each aircraft weight over the course of 180,000 lbs of fuel burn. This type of cost-indexed cruise data found in the United Airlines manual requires the aircraft to constantly ascend to a higher altitude per 20,000 lbs of fuel burned in order to fly in the most cost-effective manner. Although some form of a step-cruise typically occurs in flight, the optimum case is shown in this paper, and seldom occurs on actual flights.

With changes in aircraft capability found in parametric aircraft sizing studies, more options will exist for the aircraft at airports and in airspace, having indirect impacts on the capacity and throughput of the NAS. The effects will reach beyond fuel efficiency and flight performance optimization. If CNRP aircraft flew today, several impacts on the NAS would be feasible. Higher cruise altitudes as compared to the highest initial M_{AT} aluminum aircraft mean that CNRP aircraft would provide more options for optimizing airspace. Airports would see the benefits of increased throughput, with aircraft turning off on earlier taxiways due to decreased runway length requirements and closer in-trail spacing, and allow larger aircraft to operate at smaller airports due to their reduced runway length requirements.

The high-level analysis presented provides a glimpse of the potential impacts on an aircraft from implementation of CNRP in the airframe. The calculations presented consider only a few effects a material influenced by nanotechnology might have on aircraft structures, their efficiency, and performance.

Section 6

Conclusion

With its high strength to weight ratio, CNRP fits ideally in aerospace applications. This study analyzes the use of carbon nanotubes as a molecular fiber in a composite material and illustrates the potential impact of CNRP composites through analysis of a current 747-400 airframe, where the volume of structural aluminum is replaced with an equivalent volume of CNRP with no changes to the airframe design.

CNRP material constructed with 60-70% SWNT shows slight improvements over current graphite epoxy composites used in airframes, especially in specific strength (see Tables 2-1 and 2-3). The average mass savings of CNRP structured over aluminum structured 747-400 is 10.07%.

The average increase in predicted fuel efficiency from each of the CNRP structured aircraft categories is 11.2%, with other notable gains in predicted range, flight duration, and increased cruise altitude. Cruising at 39,000 ft, traverses 4,350 nautical miles, and consumes fuel 12-24% more efficiently than current 747-400s for a Trans-Continental US flight, the low mass CNRP aircraft provide the most interesting results in the analysis. During that flight, it conserves 3,000-5,300 gallons of fuel and saves $2,700-$4,770 in fuel cost. In terms of flight performance, CNRP aircraft of all SWNT volume fraction and range performed approximately equivalent to the low mass aluminum 747-400. A similar trend is found in the wake vortex analysis, with CNRP structured 747-400 exhibiting a 5% reduction in vortex root circulation.

List of References

1. Shackelford, J. F., 2000, *Introduction to Materials Science for Engineers,* 5th Ed., Upper Saddle River: Prentice Hall.
2. Ijima, S., 1991, "Helical Microtubules of Graphitic Carbon," *Nature*, Vol. 354, pp. 56-58.
3. Yu, M. F., B. S. Files, S. Arepalli, and R. S. Ruoff, 2000, "Tensile Loading of Ropes of Single Wall Carbon Nanotubes and Their Mechanical Properties," *Physical Review Letters,* Vol. 84, pp. 5552-5555.
4. Krishnan, A., E. Dujardin, T. W. Ebbesen, P. N. Yianilos, and M. M. J. Treacy, 1998, "Young's Modulus of Single-Walled Nanotubes," *Physical Review B*, Vol. 58, pp. 14013-14019.
5. "Boeing 747-400 Fun Facts, Parts," http://www.boeing.com/commercial/747/family/pf/pf_facts.html.
6. Sweetman, B., "Boeing 7E7 Composites," *Paris Air Show 2003,* AviationNow Show News Online, Aviation Week, www.aviationweek.com/shownews/03paris/topstor08.htm.
7. "Boeing's New 7E7 to be 50% Composite," Newsroom, Netcomposites, www.netcomposites.com/news.asp?1867.
8. Chang, K., 2002, "It Slices! It Dices! Nanotube Struts Its Stuff," *New York Times,* Boston, pp. 1-3.
9. Pipes, R. B., S. J. V. Frankland, P. Hubert, and E. Saether, November 2002, *Self-Consistent Physical Properties of Carbon Nanotubes in Composite Materials*, NASA Langley Research Center, Hampton, Virginia, NASA/CR-2002-212134.
10. Qian, D., G. J. Wagner, W. K. Liu, M. F. Yu, and R. S. Ruoff, "Mechanics of Carbon Nanotubes," *Applied Mechanics Review*, Vol. 55, pp. 495-533.
11. Köhler, T., and F. Vollrath, 1995, "Thread Boimechanics in the Two Orb-Weaving Spiders Araneus Diadematus (Araneae, Araneidae) and Uloboris Walckenaerius (Araneae, Uloboridae)," *Journal of Experimental Zoology*, Vol. 271, pp. 1-17.
12. Penumadu, D., A. Dutta, G. M. Pharr, and B. Files, 2003, "Mechanical Properties of Blended Single Wall Carbon Nanotube Composites," *Journal of Materials Research*, Vol. 18, No. 8, pp. 1-3.
13. Hadjiev, V. G., M. N. Iliev, S. Arepalli, P. Nikolaev, and B. S. Files, 2001, "Raman Scattering Test of Single-Wall Carbon Nanotube Composites," *Applied Physics Letters*, Vol. 78, No. 21, pp. 1-3.

14. Kumar, S. et al., 2002, "Synthesis, Structure, and Properties of PBO/SWNT Composites," *Macromolecules*, Vol. 35, pp. 9039-9043.

15. Saito, R., M. Fujita, G. Dresselhaus, M. S. Dresselhaus, "Electronic-Structure of Chiral Graphene Tubules," *Applied Physics Letters*, Vol. 6, pp. 2204-2206.

16. Louie, S. G., "Electronic Properties, Junctions, and Defects of Carbon Nanotubes," *Carbon Nanotubes, Topics in Applied Physics 80*, Edited by Dresselhaus G., and P. Avouris, 2001, Apringer-Verlag, Heidelberg, pp. 113.

17. White, C. T., and T. N. Todorov, 1998, "Carbon Nanotubes as Long Ballistic Conductors," *Nature*, Vol. 393, pp. 240-242.

18. Frank, S. P., P. Poncharal, Z. L. Wang, W. A. deHeer, 1998, "Carbon Nanotube Quantum Resistors," *Science*, Vol. 280, pp. 1744-1746.

19. Gao, G., T. Çagin, and W. A. Goddard, 1998, "Energetics, Structure, Mechanical and Vibrational Properties of Single-Walled Carbon Nanotubes," Nanotechnology, Vol. 9, pp. 184-191.

20. Frankland, S. J. V., T. Bandorawalla, and T. S. Gates, 2003, "Calculation of Non-Bonded Forces Due to Sliding of Bundled Carbon Nanotubes," Paper presented at 44th AIAA/ASME/AHS Structures, Structural Dynamics, and Materials Conference, Norfolk, Virginia.

21. Yu, M. F., O. Lourie, M. J. Dyer, K. Moloni, T. F. Kelly, and R. S. Ruoff, 2000, "Strength and Breaking Mechanism of Multiwalled Carbon Nanotubes under Tensile Load," *Science*, Vol. 287, pp. 637-640.

22. Yu, M. F., B. I. Yakobson, and R. S. Ruoff, 2000, "Controlled Sliding and Pullout of Nested Shells in Individual Multiwalled Carbon Nanotubes," *Journal of Physical Chemistry B*, Vol. 104, pp. 8764-8767.

23. Dow, 2003, "Dow HDPE 65053N High Density Polyethylene," Vol. 2003: MatWeb.

24. Chesnokov, S. A., V. A. Nalimova, A. G. Rinzler, R. E. Smalley, and J. E. Fischer, 1999, "Mechanical Energy Storage in Carbon Nanotube Springs," *Physical Review Letters*, Vol. 82,pp. 343-346.

25. Agarwal, B. D., and L. J. Broutman, 1990, *Analysis and Performance of Fiber Composites*, 2nd Ed., New York: John Wiley & Sons, Inc.

26. Reynolds, A., August 2001, Final Briefing of The MITRE Corporation NanoSystems Group.

27. Kollár, L. P., and G. S. Springer, 2003, *Mechanics of Composite Structures*, Cambridge: Cambridge University Press.

28. "Properties and Selection: Irons, Steels, and Height Performance Alloys," 1990, *Metals Handbook*, 10th Ed., Vol. 1, Materials Park, Ohio: ASM International.

29. *Materials Properties Handbook: Titanium Alloys*, 1994, Edited by Boyer, R., G. Welsch, and E. W. Collings, Materials Park, Ohio: ASM International.

30. Raymer, D. P., 1999, *Aircraft Design: A Conceptual Approach*, 3rd Ed., Reston: American Institute of Aeronautics and Astronautics.

31. "Properties and Selections: Nonferrous Alloys and Special-Purpose Materials," 1990, *Metals Handbook*, 10th Ed., Vol. 2, Materials Park Ohio: ASM International.

32. Ajayan, P. M., L. S. Schandler, C. Giannaris, and A. Rubio, 2000, "Single-Walled Carbon Nanotube Composites: Strength and Weakness," *Advanced Materials*, Vol. 12, pp. 750-753.

33. Sandler, J., M. S. P. Shaffer, T. Prasse, W. Bauhofer, K. Schulte, and A. H. Windle, 1999, "Development of a Dispersion Process for Carbon Nanotubes in an Epoxy Matrix and the Resulting Electrical Properties," *Polymer*, Vol. 40, pp. 5967-5971.

34. Schandler, L. S., S. C. Giannaris, and P. M. Ajayan, "Load Transfer in Carbon Nanotube Epoxy Composites," *Applied Physics Letters*, Vol. 73, pp. 3842-3844.

35. Qian, D., E. C. Dickey, R. Andrews, and T. Rantell, 2000, "Load Transfer and Deformation Mechanisms in Carbon Nanotube-Polystyrene Composites," *Applied Physics Letters*, Vol. 76, pp. 2868-2870.

36. Vergano, D., 2003, "Researchers Spin Super-Powerful Fiber," *USA Today*.

37. Yoon, C. K., 2003, "Those Intriguing Nanotubes Create the Toughest Fibers Known," *New York Times*, pp. D3.

38. Dalton, A. B., et al., 2003, "Super-Tough Carbon-Nanotube Fibres, *Nature*, Vol. 423, pp. 703.

39. Gates, T. S., and J. A. Hinkley, March 2003, *Computational Materials: Modeling and Simulation of Nanostructrued Materials and Systems*, NASA Langley Research Center, Hampton, Virginia, NASA/TM-2003-212163.

40. The Boeing Company, *Airport Manual for 747-400*, D6-58326-1.

41. Asselin, M., 1997, "An Introduction to Aircraft Performance," Reston, Virginia: AIAA.

42. *United Airlines B-747-400 Flight Handbook*, "Four Engine Cost-Indexed Cruise," 21 September 1990, pp. C-6.1, C-6.2; 1 May 1992, "Four Engine Holding Speed and Fuel Flow," p. C-9.

43. *FAA, Air Traffic Control Order 7110.65N*, 2002, Federal Aviation Administration.

44. “Traffic and Financial Reports, “2001, U. S. Department of Transportation, Form 41: Financial Data.

45. Jenkinson, L. R., P. Simpkin, and D. Rhodes, *Civil Jet Aircraft Design*, 1999, Oxford: Butterworth Heinemann.

46. Saffman, P. G., *Vortex Dynamics*, 1992, Cambridge: Cambridge University Press.

47. Proctor, F. H., and G. F. Switzer, 2000, Numerical Simulation of Aircraft Trailing Vortices,” September 2000, presented at the *American Meteorological Society’s 9th Conference on Aviation, Range, and Aerospace Meteorology*, Orlando.

48. Gerz, T., F. Holzaepfel, and D. Darracq, April 2001, “Aircraft Wake Vortices – A Position Paper,” *WakeNet*.

Glossary

CAASD	Center for Advanced Aviation System Development
C_h	Chiral Vector
CNRP	Carbon Nanotube Reinforced Polymer
EPR	Engine Pressure Ration
FAA	Federal Aviation Administration
GPa	Giga Pascal
HDPE	High Density Polyethylene
M_{AT}	Mass at Takeoff
M_F	Maximum Fuel Load
M_L	Maximum Payload
MOM	Method of Mixtures
MPa	Mega Pascal
M_{TO}	Mass at Takeoff
MWNT	Multi-Walled Nanotubes
NAM	Nautical Miles
NAS	National Airspace System
OEW/M_{OE}	Operating Empty Weights
SWNT	Single-Walled Carbon Nanotube
TAS	True Airspeed
TPa	Tera Pascal
T_R	Thrust Required
V_{max}	Maximum Velocity
V_{min}	Minimum Velocity
V_{stall}	Stall Speed
ZFW	**Zero Fuel Weight**